Molecular-Level Dispersion of Graphene into Poly(vinyl alcohol) and Effective Reinforcement of their Nanocomposites

By *Jiajie Liang, Yi Huang,* Long Zhang, Yan Wang, Yanfeng Ma, Tianyin Guo,* and *Yongsheng Chen**

Despite great recent progress with carbon nanotubes and other nanoscale fillers, the development of strong, durable, and cost-efficient multifunctional nanocomposite materials has yet to be achieved. The challenges are to achieve molecule-level dispersion and maximum interfacial interaction between the nanofiller and the matrix at low loading. Here, the preparation of poly(vinyl alcohol) (PVA) nanocomposites with graphene oxide (GO) using a simple water solution processing method is reported. Efficient load transfer is found between the nanofiller graphene and matrix PVA and the mechanical properties of the graphene-based nanocomposite with molecule-level dispersion are significantly improved. A 76% increase in tensile strength and a 62% improvement of Young's modulus are achieved by addition of only 0.7 wt% of GO. The experimentally determined Young's modulus is in excellent agreement with theoretical simulation.

1. Introduction

Nanocomposites, used as nanoscale fillers at low loading, have the potential to match or exceed the performance of significant quantities of conventional composite filler. However, maximal mechanical enhancement can only be achieved when the ''nanofiller'' is dispersed homogeneously, or best at the molecular level, in the matrix and the external load is efficiently transferred via a strong interaction at the interface between the filler and the matrix. At present, although nanocomposites employing carbon-based reinforcement materials are dominated by carbon nanotubes, the intrinsic bundling of carbon nanotubes, their intrinsic impurities from catalysts, and their high cost have been hampering their application. Theoretical[1] and experimental[2] results show that single-layered two-dimensional (2D) graphene sheets are the strongest materials developed thus far. Due to their extraordinary electronic and thermal properties, nanoscale materials based on individual graphene sheets have recently attracted tremendous attention.[3–9] Great strides have been made in the use of solution-processable graphene materials for highly conducting composite,[7] transparent electrode,[10] and photovoltaic device[11,12] applications.

Perfect graphene does not exist naturally, but bulk and solution-processable functionalized graphene materials including graphene oxide (GO) can now be prepared.[1,8,13–16] For GO, oxygen-containing functional groups including hydroxyls, epoxides, diols, ketones and carboxyls significantly alter the van der Waals interactions between the layers of graphene and impart the desired characteristic of water solubility.[1,8,16,17] These chemical functionalizations have been found to be a feasible and effective means for improving the dispersion of graphene. Additionally, functional side groups bound to the surface of graphene sheets may improve interfacial bonding between the graphene and the matrix similarly to that observed for functionalized carbon nanotube-based nanocomposites.[18–20] Thus, by combining remarkable mechanical properties and low costs, 2D graphene sheets are expected to offer a promising nanoscale filler for the next generation of nanocomposite materials. In particular, some prominent reports have explored the intriguing applications (such as organic conductive films and lithium-ion batteries) of GO/polymer nanocomposites fabricated through layer-by-layer self-assembly.[21,22] However, GO is not quite ready for application as a reinforcement material. Before implementation of high-performance graphene-based nanocomposites can be achieved, a number of practical challenges must be addressed. Firstly, truly homogeneous dispersion of graphene sheets in their host polymer matrix must be achieved; currently, intrinsic van der Waals interactions between layers of graphene sheets easily leads to agglomeration, which results in insolubility as in the case of bundled carbon nanotubes.[19] Individual carbon nanotube dispersion can barely be achieved even for functionalized carbon nanotubes[19] or by using surfactants.[23] Such agglomerations lower the effectiveness of nanofillers for reinforcement, as maximal load transfer and lowest filling load can only be achieved when the nanofiller is dispersed at the molecular level in the polymer matrix. In the case of graphene, since GO can be dispersed

[*] Dr. Y. Huang, Prof. Y. Chen, J. J. Liang, L. Zhang, Y. Wan, Dr. Y. F. Ma, Prof. T. Y. Guo
Key Laboratory of Functional Polymer Materials and Centre of Nanoscale Science and Technology
Institute of Polymer Chemistry, College of Chemistry, Nankai University
300071, Tianjin (P. R. China)
E-mail: yihuang@nankai.edu.cn; yschen99@nankai.edu.cn

DOI: 10.1002/adfm.200801776

at the individual sheet level in water, it is possible to achieve a truly molecular-level dispersion of graphene if water is used as the common solvent for both graphene and the polymer matrix. Additionally, implementation of high-performance graphene-based nanocomposites requires maximal interfacial adhesion between graphene and the surrounding polymer matrix, as well as effective load transfer. We believe that the most effective approach is probably to use the force of hydrogen bonding (H-bonding), which is arguably the strongest van der Waals interaction, in the absence of direct chemical bonding between the filler and matrix via surface molecular engineering. Thus, selection of the matrix is equally important for achieving efficient load transfer. The ease of processing and environmental issues must also be considered for practical use.

Taking these considerations into account, we show here a simple and environmentally friendly preparation of graphene/poly(vinyl alcohol) (PVA) nanocomposites by incorporating GO into a PVA matrix using water as the processing solvent. Efficient load transfer was found between the graphene nanofiller and the PVA matrix, and significant reinforcement was observed for these nanocomposites. A 76% increase in tensile strength and a 62% improvement of Young's modulus were achieved by addition of only 0.7 wt% GO. Furthermore, excellent agreement was found between the experimental nanocomposite modulus data and a Halpin–Tsai theoretical prediction.[24–27] These results demonstrate that effective load transfer across the graphene–PVA interface occurred due to molecule-level dispersion and strong H-bonding.[19,25,28] Finally, this simple solution-mixing method is environmentally friendly as it uses only water as the processing solvent.

2. Results and Discussion

2.1. Dispersion of Individual GO Sheets into PVA

GO used in this work was prepared from graphite by the modified Hummers method[29,30] as described elsewhere.[29] Well-dispersed graphene/PVA nanocomposites were fabricated through a simple solution-mixing method as described in the experimental section. GO, which contains many oxygen-containing functional groups, can be dispersed very well in water at the level of individual sheets.[8] Figure 1a displays a typical tapping-mode atomic-force microscopy (AFM) image of GO sheets deposited onto a mica substrate from an aqueous dispersion. Analysis of a large number of AFM images revealed most GO sheets had heights of about 0.8 nm, which is characteristic of a fully exfoliated graphene sheet,[7–9,15,30] and lengths in the range of 2–3 μm. Transmission electron microscopy (TEM) was also employed to determine the existence of individual graphene sheets in water. The TEM images shown in Figure 1b show that graphene was fully exfoliated into individual sheets by ultrasonic treatment. PVA, which is also water-soluble due to its many hydroxyl groups, was expected to have truly homogenous co-dispersion with graphene at the molecular level. Furthermore, potential H-bonding between GO and PVA could lead to enhanced interfacial adhesion and mechanical performance of the nanocomposite.[19] The dispersion state of GO sheets in the PVA matrix was detected by scanning electron microscopy

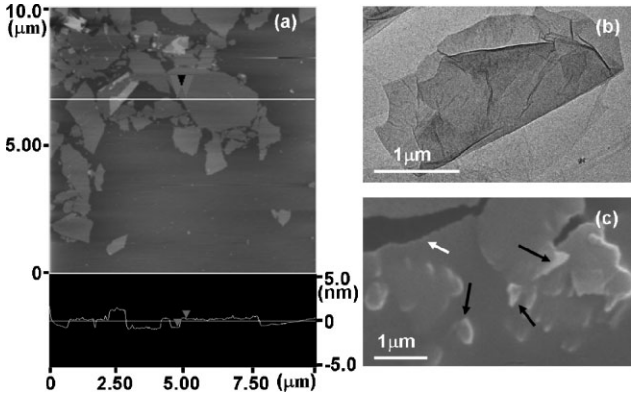

Figure 1. Characterization of individual graphene sheets and dispersion state of GO in the polymer matrix. a) Typical tapping-mode AFM image of graphene sheets deposited on mica substrate from an aqueous dispersion; the height difference between the arrows is ~0.8 nm, indicating the typical height of an individual GO sheet. b) Typical TEM image of an individual graphene sheet in water solution. c) SEM cross-sectional image of graphene/PVA nanocomposites with GO concentration of 0.7 wt%. The black arrows indicate GO sheets, and the white arrow points to a fracture.

(SEM), and Figure 1c shows a typical SEM image of the cross section of the graphene/PVA nanocomposite with 0.7 wt% loading. The GO sheets are clearly well-dispersed in the PVA matrix.

X-ray diffraction (XRD) is an important tool for determining whether graphene-based sheets are indeed present as individual graphene sheets in the nanocomposites. Figure 2 shows the XRD patterns of GO (curve a), graphene/PVA nanocomposite with 0.5 wt% loading of GO (curve b) and pure PVA (curve c). The typical diffraction peak of GO was observed at about $2\theta = 10.9^\circ$ (Fig. 2a) and the diffraction peak of pure PVA appeared at $2\theta = 19.6^\circ$ (Fig. 2c). However, after GO was dispersed into the PVA matrix, the XRD pattern of the graphene/PVA nanocomposite (Fig. 2b) only showed the PVA diffraction peak from PVA; the diffraction peak of GO disappeared. The XRD results clearly demonstrate that GO was fully exfoliated into individual graphene sheets in the polymer matrix and that the regular and periodic structure of graphene disappeared.[1,31–33] Nanocomposites with other GO loadings gave similar XRD results.

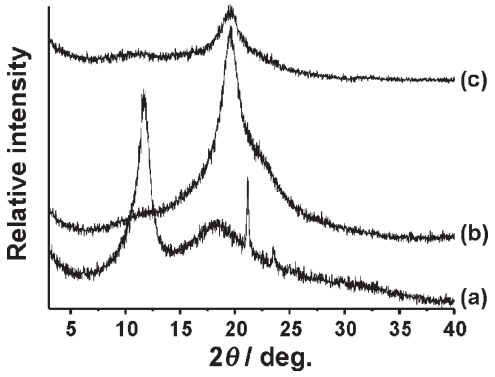

Figure 2. XRD patterns. a) GO, b) graphene/PVA nanocomposite with 0.5 wt% loading of GO, and c) pure PVA.

2.2. Mechanical Properties of Graphene/PVA Nanocomposites

It was expected that the mechanical performance of the nanocomposite would be significantly enhanced by the large aspect ratio of the graphene sheets, the molecular-level dispersion of the graphene sheets in PVA matrix, and strong interfacial adhesion due to H-bonding between graphene and the PVA matrix. The representative stress-strain relationship for graphene/PVA nanocomposites within the tested range of GO weight fractions is given in Figure 3a. The mechanical performance of the graphene/PVA nanocomposite was significantly increased as compared to that of the pure PVA matrix. For example, with only 0.7 wt% (0.41 vol%) GO, the tensile strength increased by 76% from 49.9 to 87.6 MPa (Fig. 3a), and the Young's modulus increased by 62% from 2.13 to 3.45 GPa (Fig. 3b). The breaking elongation of the nanocomposites was decreased as compared to pure PVA (Fig. 3a). Because the aspect ratio and dispersion state of graphene were similar in nanocomposites with different GO loading, the enhanced mechanical properties are believed to arise from the strong interaction between graphene and the PVA matrix.[24]

The Halpin–Tsai model, which is widely used[24,26,27,34] for predicting the modulus of unidirectional or randomly distributed filler-reinforced nanocomposites, was used in our work to simulate the modulus of the graphene/PVA nanocomposites. For randomly oriented or unidirectional graphene sheets in the polymer matrix, the nanocomposite modulus E_c and $E_{||}$ are given by

$$E_c = E_m\left[\frac{3}{8}\frac{1+\eta_L\xi V_c}{1-\eta_L V_c}+\frac{5}{8}\frac{1+2\eta_T V_c}{1-\eta_T V_c}\right] \quad (1)$$

$$E_{||} = E_m\left[\frac{1+\eta_L\xi V_c}{1-\eta_L V_c}\right] \quad (2)$$

$$\eta_L = \frac{(E_g/E_m)-1}{(E_g/E_m)+\xi} \quad (3)$$

$$\eta_T = \frac{(E_g/E_m)-1}{(E_g/E_m)+2} \quad (4)$$

$$\xi = 2\alpha_g/3 = 2l_g/3t_g \quad (5)$$

where E_c and $E_{||}$ represent the Young's modulus of the nanocomposite with randomly distributed GO and the Young's modulus of the nanocomposite with GO aligned parallel to the surface of the sample film, respectively. E_g and E_m are Young's modulus of the GO and the polymer matrix. α_g, l_g, and t_g refer to the aspect ratio, length and thickness of the graphene oxide sheet, and V_c is the volume fraction of GO in the nanocomposites. The Young's modulus of the chemically reduced graphene oxide sheet was previously measured as around 0.25 TPa,[9] which may approach to that of the graphene and is used here. The Young's modulus of pure PVA was 2.13 GPa from the experimental data. The density of the PVA matrix is 1.3 g cm^{-3}, and the density of GO is 2.2 g cm^{-3}. The statistical average l_g and t_g of graphene oxide sheet were about 2.5 μm and 0.8 nm, respectively, as determined by AFM analysis. Substituting these parameters into Equations 1 to 5, the Young's modulus of the nanocomposite was calculated under two hypotheses: i) GO aligned parallel to the surface of the sample film and ii) GO randomly dispersed as 3D network throughout the polymer matrix. As shown in Figure 3b, good agreement was found between the experimental data obtained for graphene/PVA nanocomposites and the theoretical simulation results under the hypothesis that GO is aligned parallel to the surface of the nanocomposite film. This consistency indicates that external tensile loads were successfully transmitted to the GO filler across the graphene–PVA interface via strong interfacial interactions,[25,28] and presumably the graphene oxide sheets prefer to align parallel to the surface of the sample film within the nanocomposites,[28] which requires further investigation.

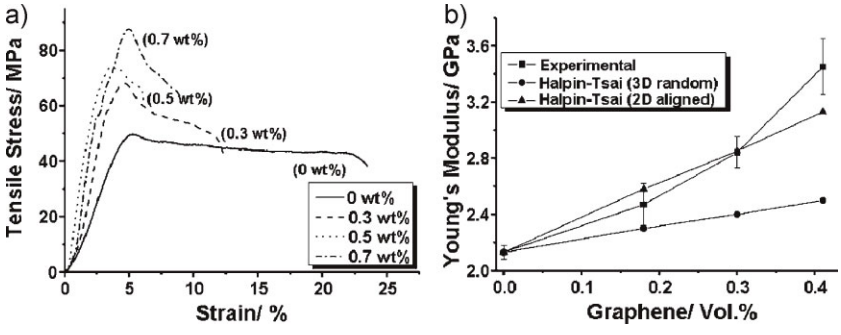

Figure 3. a) Representative stress-strain behavior for graphene/PVA nanocomposites with different GO weight loadings. With only 0.7 wt% GO, the tensile strength of the nanocomposite increased by 76% from 49.9 to 87.6 MPa. b) experimental Young's modulus of the nanocomposite films, calculated data derived from the Halpin–Tsai model under the hypothesis that GO sheets randomly dispersed as 3D network throughout the polymer matrix, and calculated data derived from the Halpin–Tsai model under the hypothesis that GO sheets aligned parallel to the surface of the composite film.

We believe that the effective load transfer was due to strong H-bonding interactions between oxygen-containing groups (e.g., hydroxyls, carboxyls and epoxides) of the graphene sheets and the hydroxyl groups of the PVA chains. These H-bonding interactions were expected to affect the mobility of PVA polymer chains. To confirm this, differential scanning calorimetry (DSC) was used to compare the glass-transition temperature (T_g) of pure PVA with that of the graphene/PVA nanocomposite as shown in Figure 4a. The T_g of graphene/PVA nanocom-

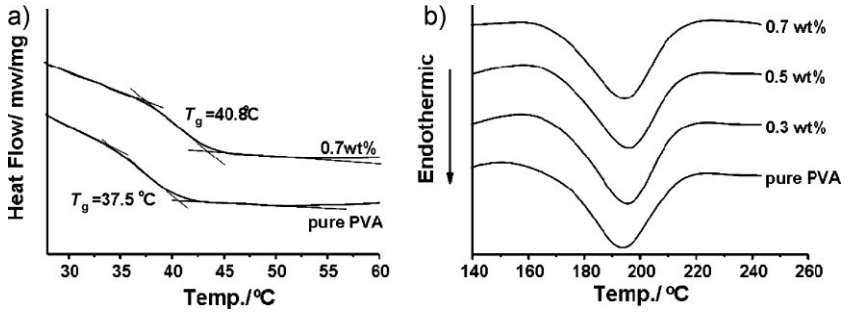

Figure 4. a) Glass-transition temperature measurement of pure PVA and graphene/PVA nanocomposite with 0.7 wt% GO loading. The T_g of graphene/PVA nanocomposite with 0.7 wt% GO loading was 3.3 °C higher than that of the pure PVA matrix. T_g was obtained by DSC measurement. b) Melting peaks of pure PVA and graphene/PVA nanocomposites with GO loadings of 0.3, 0.5, and 0.7 wt%. DSC was used to measure the melting enthalpy of the samples and the melt peaks were in the range of 160–220 °C.

Table 1. Crystallinity and melting enthalpy of pure PVA and graphene/PVA nanocomposites with GO loadings of 0.3 wt%, 0.5 wt%, and 0.7 wt%. There was no obvious change of PVA crystallinity.

Samples	ΔH_m (J g^{-1})	χ_c
pure PVA	23.6 ± 1.4	17.0 ± 1
PVA/GO/0.3 wt %	25.4 ± 0.9	18.3 ± 0.6
PVA/GO/0.5 wt %	24.1 ± 1.1	17.4 ± 0.8
PVA/GO/0.7 wt %	23.9 ± 2.0	17.2 ± 1.4

posite with 0.7 wt% GO loading increased from 37.5 to 40.8 °C. This T_g increase indicates that the polymer chains were indeed constrained by the H-bonding interaction, an effect also demonstrated in other reports.[19,35,36]

Since PVA is a semicrystalline polymer, its mechanical properties strongly depend on the degree of its crystallinity. To demonstrate that the mechanical enhancement of graphene/PVA nanocomposites was not due to a change in crystallinity, DSC was used to measure the melting enthalpy of pure PVA and graphene/PVA nanocomposites. For pure PVA and three nanocomposite samples, the melt curves are shown in Figure 4b. The melting peaks had similar patterns and all were in the same range of 160–220 °C. This indicates that PVA had similar crystallinity (χ_c) in all samples, calculated as follows:

$$\chi_c = \frac{\Delta H_m}{\Delta H_0} \quad (6)$$

where ΔH_m is the measured melting enthalpy (from DSC) and ΔH_0 is the enthalpy of pure PVA crystal (138.6 J g^{-1}).[37,38] As shown in Table 1, no obvious change of PVA crystallinity was observed in graphene/PVA nanocomposites containing 0.3–0.7 wt% GO. Therefore, the significantly increased strength and modulus of the graphene/PVA nanocomposites cannot be attributed to changes in crystallinity. Similar results have been demonstrated for carbon-nanotube-based nanocomposites.[19,23]

In general, load transfer depends strongly on the interfacial interaction between the filler and the wrapped polymer matrix.[39] As discussed above, the oxygen-containing groups attached to the surface of graphene can generate strong interactions with the PVA matrix through H-bonding. Furthermore, the molecular-level dispersion of graphene sheets in the PVA matrix and the large aspect ratio of graphene are also favorable for stress transfer across the graphene-PVA interface. As a result, significant enhancement of the tensile stress and modulus of the nanocomposites was achieved.

2.3. Thermal Properties of Graphene/PVA Nanocomposites

It is interesting to note that the mechanical performance of graphene/PVA nanocomposites was not the only aspect of the composites enhanced; the thermal stability of these materials was also mildly increased even with the low loadings of GO used. Thermogravimetric analysis (TGA) and corresponding differential thermogravimetric analysis (DTG) results for pure PVA and graphene/PVA nanocomposite with 0.7 wt% GO loading are shown in Figure 5. Both pure PVA and its nanocomposite decompose in a two-step process, and the TGA curve of the nanocomposite was shifted toward a higher temperature when compared to that of pure PVA. The onset temperature of degradation for the nanocomposite was about 3 °C higher at 0.7 wt% GO loading. The peak temperature (T_p) of the DTG curve represents the temperature at which the maximum weight loss rate was reached, as shown in Figure 5b. The T_p of the nanocomposite appeared at about 316.5 °C and 428.6 °C and was increased by about 5.5 °C and 2 °C, respectively, as compared to pure PVA. Though the values are low than that of the functionalized graphene sheets or expanded graphite based polymer nanocomposites,[35] these results still indicate that addition of GO at low concentrations somewhat improved the thermal stability of the nanocomposite.

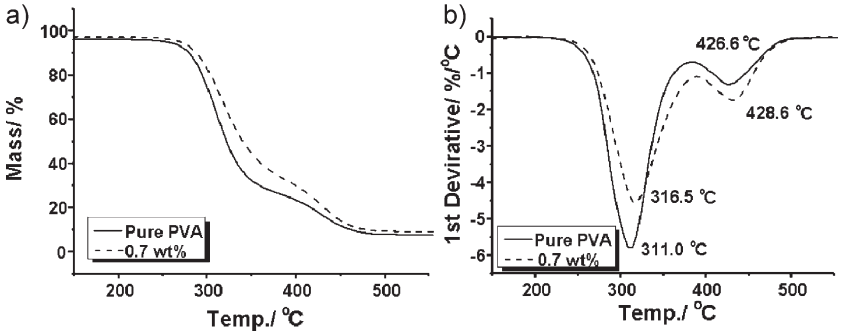

Figure 5. a) TGA curves of pure PVA and graphene/PVA composite with 0.7 wt% GO loading and b) corresponding DTG curves of pure PVA and graphene/PVA nanocomposite with 0.7 wt% GO loading.

3. Conclusions

In conclusion, we have prepared the first PVA nanocomposite to use graphene as a mechanical reinforcement material. The graphene/PVA nanocomposites can be fabricated using a simple and environmentally friendly method with water as the processing solvent. Significant enhancement of the mechanical properties of graphene/PVA nanocomposites was obtained at fairly low concentrations of graphene oxide. A 76% increase in tensile strength and a 62% improvement of Young's modulus were achieved by the addition of only 0.7 wt% graphene oxide. Furthermore, the agreement between the experimental tensile modulus data and the values predicted by the Halpin–Tsai model indicates that the external tensile loads were successfully transferred to the graphene sheets across the graphene–PVA interface via strong hydrogen bonding. It should be emphasized that this hydrogen-bonding approach may have wide-reaching implications for the preparation of other multifunctional nanocomposite materials. Additionally, the achievement of significant mechanical enhancement with such low loading indicates that matrix properties could be maintained for multifunctional graphene nanocomposite materials. Collectively, we have shown that a water solution-based method can be used to generate graphene/PVA nanocomposites with excellent mechanical properties; the abundant supply of graphite and the processability of functionalized graphene sheets with high purity may allow the ready implementation of graphene-based materials as effective nanofillers for many practical nanocomposite applications.

4. Experimental

Raw Materials: Graphite was obtained from Qingdao Huarun graphite Co., LTD with a particle size of 20 μm. Poly(vinyl alcohol) (PVA) was purchased from Alfa Aesar (86–89% hydrolyzed, low molecular weight).

Fabrication of Nanocomposites: Graphene oxide (GO) used as the reinforcement filler was prepared from graphite by the modified Hummers method [29,30]. The synthesis procedure for a typical well-dispersed graphene/PVA nanocomposite (0.7 wt%) was as follows: GO (7 mg) was dispersed in distilled water (3 mL) in an ultrasonic bath (Gongyi Yuhua Instrument Co., LTD, Model: KQ400B, 400 W) for 30 min at room temperature to yield a clear solution. In this process, GO was completely exfoliated down to individual sheets to form a stably dispersed GO/H_2O solution [8]. Meanwhile, PVA (1 g) was dissolved in distilled water (7 mL) at 90 °C and the solution was subsequently cooled to room temperature. After the PVA/H_2O solution had cooled to around 40 °C, the GO aqueous dispersion was gradually added to the PVA solution and sonicated for an additional 30 min at room temperature. Finally, this homogeneous graphene/PVA solution was poured into a Teflon Petri dish and kept at 60 °C for film formation until its weight equilibrated. This film was peeled off of the substrate for mechanical testing. A series of PVA/graphene nanocomposite films with different GO loadings were similarly prepared.

Characterization: Typical tapping-mode atomic-force microscopy (AFM) measurements were performed using Multimode SPM from Digital Instruments with a Nanoscope IIIa Controller. Samples for AFM images were prepared by depositing a dispersed GO/H_2O solution (0.2 mg mL^{-1}) onto a freshly cleaved mica surface and allowing them to dry in air. Transmission electron microscopy (TEM) was performed using a Philips T20ST electron microscope at an acceleration voltage of 200 kV. The GO/H_2O solution was dropped onto carbon-coated copper grids (mesh size 300) and allowed to dry under ambient conditions. Scanning electron microscopy (SEM) was performed on a Hitachi S-3500N scanning electron microscope with acceleration voltage of 20 kV. Samples were prepared by immersing the films in liquid nitrogen for 10 min before fracture. The fracture surfaces were coated with gold before analysis. X-ray diffraction (XRD) measurements were carried out using a Rigaku D/Max-2500 diffractometer with Cu-Kα radiation. The glass-transition temperature (T_g) and degree of crystallinity of the samples were investigated by differential scanning calorimetry (DSC) using a NETZSCH STA-409PC instrument. Thermogravimetric analysis (TGA) and differential thermogravimetric analysis (DTG) were also carried out using the same apparatus. The heating rate was 5 °C min^{-1}, and approximately 15 mg of each sample were measured in an aluminum crucible under N_2.

Mechanical Measurement: The mechanical properties of PVA/graphene nanocomposites were measured by a universal tensile testing machine (KNM 500-10 test metric, U.K) at 22 °C with 50% relative humidity. The extension rate was 5 mm min^{-1} and the load cell was 250 N with a gauge length of ~20 mm. All samples were cut into strips of ~40 mm × 6 mm × 0.04 mm using a razor blade. The width and thickness of each strip were measured utilizing a low torque digital micrometer. In all cases, more than five samples were tested from which the mean and standard deviation were calculated.

Acknowledgements

The authors gratefully acknowledge the financial support from the NSFC (#20774047), MOST (#2006CB932702), MOE (#708020) of China and NSF of Tianjin City (#07JCYBJC03000 and #08JCZDJC25300).

Received: December 1, 2008
Published online:

[1] M. J. McAllister, J. L. Li, D. H. Adamson, H. C. Schniepp, A. A. Abdala, J. Liu, M. Herrera-Alonso, D. L. Milius, R. Car, R. K. Prud'homme, I. A. Aksay, *Chem. Mater.* **2007**, *19*, 4396.
[2] C. G. Lee, X. D. Wei, J. W. Kysar, J. Hone, *Science* **2008**, *321*, 385.
[3] D. A. Dikin, S. Stankovich, E. J. Zimney, R. D. Piner, G. H. B. Dommett, G. Evmenenko, S. T. Nguyen, R. S. Ruoff, *Nature* **2007**, *448*, 457.
[4] K. S. Novoselov, A. K. Geim, S. V. Morozov, D. Jiang, Y. Zhang, S. V. Dubonos, I. V. Grigorieva, A. A. Firsov, *Science* **2004**, *306*, 666.
[5] P. Avouris, Z. H. Chen, V. Perebeinos, *Nat. Nanotechnol.* **2007**, *2*, 605.
[6] N. A. Kotov, *Nature* **2006**, *442*, 254.
[7] S. Stankovich, D. A. Dikin, G. H. B. Dommett, K. M. Kohlhaas, E. J. Zimney, E. A. Stach, R. D. Piner, S. T. Nguyen, R. S. Ruoff, *Nature* **2006**, *442*, 282.
[8] S. Stankovich, D. A. Dikin, R. D. Piner, K. A. Kohlhaas, A. Kleinhammes, Y. Jia, Y. Wu, S. T. Nguyen, R. S. Ruoff, *Carbon* **2007**, *45*, 1558.
[9] C. Gomez-Navarro, M. Burghard, K. Kern, *Nano Lett.* **2008**, *8*, 2045.
[10] S. Watcharotone, D. A. Dikin, S. Stankovich, R. Piner, I. Jung, G. H. B. Dommett, G. Evmenenko, S. E. Wu, S. F. Chen, C. P. Liu, S. T. Nguyen, R. S. Ruoff, *Nano Lett.* **2007**, *7*, 1888.
[11] Z. F. Liu, Q. Liu, Y. Huang, Y. F. Ma, S. G. Yin, X. Y. Zhang, W. Sun, Y. S. Chen, *Adv. Mater.* **2008**, *20*, 3924.
[12] X. Wang, L. J. Zhi, K. Mullen, *Nano Lett.* **2008**, *8*, 323.
[13] D. Li, M. B. Muller, S. Gilje, R. B. Kaner, G. G. Wallace, *Nat. Nanotechnol.* **2008**, *3*, 101.
[14] S. Niyogi, E. Bekyarova, M. E. Itkis, J. L. McWilliams, M. A. Hamon, R. C. Haddon, *J. Am. Chem. Soc.* **2006**, *128*, 7720.
[15] S. Stankovich, R. D. Piner, X. Q. Chen, N. Q. Wu, S. T. Nguyen, R. S. Ruoff, *J. Mater. Chem.* **2006**, *16*, 155.
[16] H. C. Schniepp, J. L. Li, M. J. McAllister, H. Sai, M. Herrera-Alonso, D. H. Adamson, R. K. Prud'homme, R. Car, D. A. Saville, I. A. Aksay, *J. Phys. Chem. B* **2006**, *110*, 8535.
[17] Y. C. Si, E. T. Samulski, *Nano Lett.* **2008**, *8*, 1679.
[18] W. D. Zhang, L. Shen, I. Y. Phang, T. X. Liu, *Macromolecules* **2004**, *37*, 256.
[19] L. Q. Liu, A. H. Barber, S. Nuriel, H. D. Wagner, *Adv. Funct. Mater.* **2005**, *15*, 975.

[20] J. N. Coleman, M. Cadek, R. Blake, V. Nicolosi, K. P. Ryan, C. Belton, A. Fonseca, J. B. Nagy, Y. K. Gun'ko, W. J. Blau, *Adv. Funct. Mater.* **2004**, *14*, 791.
[21] N. A. Kotov, I. Dékány, J. H. Fendler, *Adv. Mater.* **1996**, *8*, 637.
[22] T. Cassagneau, J. H. Fendler, *Adv. Mater.* **1998**, *10*, 877.
[23] X. F. Zhang, T. Liu, T. V. Sreekumar, S. Kumar, V. C. Moore, R. H. Hauge, R. E. Smalley, *Nano Lett.* **2003**, *3*, 1285.
[24] R. R. Tiwari, K. C. Khilar, U. J. Natarajan, *J. Appl. Polym. Sci.* **2008**, *108*, 1818.
[25] D. Qian, E. C. Dickey, R. Andrews, T. Rantell, *Appl. Phys. Lett.* **2000**, *76*, 2868.
[26] K. Kalaitzidou, H. Fukushima, H. Miyagawa, L. T. Drzal, *Polym. Eng. Sci.* **2007**, *47*, 1796.
[27] D. W. Schaefer, R. S. Justice, *Macromolecules* **2007**, *40*, 8501.
[28] J. B. Gao, M. E. Itkis, A. P. Yu, E. Bekyarova, B. Zhao, R. C. Haddon, *J. Am. Chem. Soc.* **2005**, *127*, 3847.
[29] H. A. Becerril, J. Mao, Z. Liu, R. M. Stoltenberg, Z. Bao, Y. Chen, *ACS Nano* **2008**, *2*, 463.
[30] M. Hirata, T. Gotou, S. Horiuchi, M. Fujiwara, M. Ohba, *Carbon* **2004**, *42*, 2929.
[31] X. S. Du, Z. Z. Yu, A. Dasari, J. Ma, M. S. Mo, Y. Z. Meng, Y. W. Mai, *Chem. Mater.* **2008**, *20*, 2066.
[32] X. S. Du, M. Xiao, Y. Z. Meng, A. S. Hay, *Carbon* **2005**, *43*, 195.
[33] A. Lerf, H. Heyong, M. Forster, J. Klinowski, *J. Phys. Chem. B* **1998**, *102*, 4477.
[34] J. C. Halpin, J. L. Kardos, *Polym. Eng. Sci.* **1976**, *16*, 344.
[35] T. Ramanathan, A. A. Abdala, S. Stankovich, D. A. Dikin, M. Herrera-Alonso, R. D. Piner, D. H. Adamson, H. C. Schniepp, X. Chen, R. S. Ruoff, S. T. Nguyen, I. A. Aksay, R. K. Prud'homme, L. C. Brinson, *Nat. Nanotechnol.* **2008**, *3*, 327.
[36] Z. L. Yao, N. Braidy, G. A. Botton, A. Adronov, *J. Am. Chem. Soc.* **2003**, *125*, 16015.
[37] F. T. Cerezo, C. M. L. Preston, R. A. Shanks, *Macromol. Mater. Eng.* **2007**, *292*, 155.
[38] J. X. Su, Q. Wang, R. Su, K. Wang, Q. Zhang, Q. Fu, *J. Appl. Polym. Sci.* **2008**, *107*, 4070.
[39] J. S. Jeong, J. S. Moon, S. Y. Jeon, J. H. Park, P. S. Alegaonkar, J. B. Yoo, *Thin Solid Films* **2007**, *515*, 5136.